Article

A Multichannel Screen-Printed Carbon Electrode Based on Fluorinated Poly(3-octylthiophene-2,5-diyl) and Purified Mesoporous Carbon Black Simultaneously Detects Na$^+$, K$^+$, Ca^{2+}, and NO$_2^-$

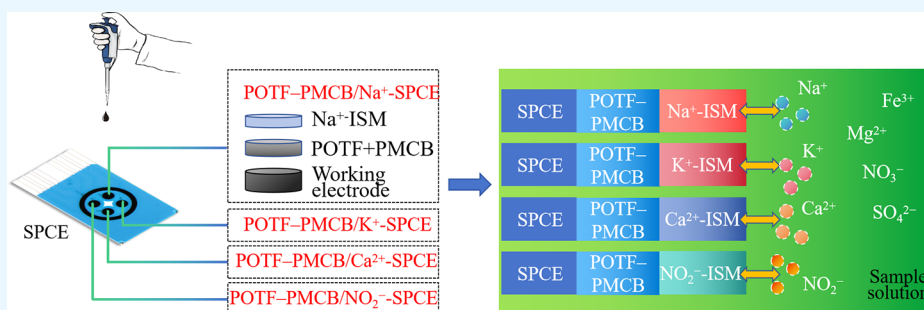Hui Bao, Jin Ye, and Yuan Zhang*

Read Online

ACCESS | Metrics & More | Article Recommendations | Supporting Information

ABSTRACT: Preparation of nanocomposites based on fluorinated poly(3-octylthiophene-2,5-diyl) (POTF) and purified mesoporous carbon black (PMCB) as the solid-contact layer of a screen-printed carbon electrode (SPCE) is proposed. POTF is used as a dispersant for PMCB. The obtained nanocomposites possess unique characteristics including high conductivity, capacitance, and stability. The SPCE based on POTF and PMCB is characterized by electrochemical impedance spectroscopy and chronopotentiometry, demonstrating simultaneous detection of Na$^+$, K$^+$, Ca^{2+}, and NO$_2^-$ ions with detection limits of $10^{-6.5}$, $10^{-6.4}$, $10^{-6.7}$, and $10^{-6.3}$ M, respectively. Water layer and anti-interference tests revealed that the electrode has high hydrophobicity, and the static contact angle is >140°. The electrode shows excellent selectivity, repeatability, reproducibility, and stability and is not easily affected by light, O$_2$, or CO$_2$.

1. INTRODUCTION

Saltiness is one of the five basic tastes, and a small amount of salt is required for human life. However, high salt intake increases health risks, especially the risk of cardiovascular disease.[1−3] The growing demand for healthier food has become a driving force in academic and industrial research, resulting in the development of low-salt foods. The addition of salt or its substitutes has a fundamental impact on the processing characteristics, sensory qualities, safety, and shelf life of food. Increased Na$^+$, K$^+$, and Ca^{2+} concentrations not only considerably affect food properties but also cause damage to the heart, nerves, and muscle.[4,5] Increased NO$_2^-$ concentrations may cause poisoning symptoms and endanger human health.[6−8] Therefore, developing methods and equipment that can analyze salt concentrations in relation to human taste are particularly important. Sensitive, portable, reliable, and cost-effective sensors are needed to monitor levels of salt and salt substitutes.

Ion-selective electrodes (ISEs), which are the most popular potential sensors at present owing to their ability to quickly and conveniently determine various ion concentrations, have been the research object of scientists worldwide for many years. Their many advantages make them applicable in agriculture,[9] the food industry,[10−12] the pharmaceutical industry,[13,14] process control, and clinical diagnosis.[15,16] However, traditional ISEs are filled with a solution that acts as the connection between the discharge electrode and ion-selective membrane (ISM), which may affect measurement accuracy and make their transportation more challenging. All-solid-state ISEs are favorable substitutes for liquid ISEs, with advantages such as long life, easy miniaturization, non-destructive testing,[17−23] process of use, transportation, and storage. Despite its many advantages, the electric double-layer capacitance between the electrode substrate and ISM of all-solid-state ISEs is small[24] while the charge transfer resistance is
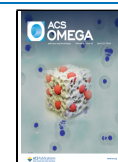
large,[25] causing the electrode to easily produce water.[26,27] The result is poor electrode stability and its potential being prone to drift. Thus, linear responses are not ideal at low-salt concentrations in the detection solution.[28,29] These disadvantages are caused by the limitation of the solid-contact layer material used for the electrode. To address these shortcomings, this study combines the high hydrophobicity of conductive polymers and the high specific surface area of carbon materials, leveraging their respective excellent properties to prepare a composite material that can be used as a solid-state contact layer in ISEs.

Poly(3-octylthiophene-2,5-diyl) (POT) is a conductive polymer known for its high hydrophobicity and ease of deposition (by drop casting or electrodeposition) onto the electrode surface with minimal involvement in side reactions. Herein, we synthesized fluorinated poly(3-octylthiophene-2,5-diyl) (POTF) containing perfluoroalkyl side chains. Fluorination further enhanced the hydrophobic properties of the POT, resulting in a more stable open-circuit potential response of the electrode. Moreover, carbon black (CB) possesses excellent conductivity and cost-effectiveness and can be uniformly dispersed. Compared to other carbon materials, CB exhibits higher stability and good resistance to interference from O_2, CO_2, and light.[30−32] Mesoporous CB (MCB) is characterized by its mesoporous structure (average pore size = 6.4 nm), high specific surface area (>200 m^2/g), and good conductivity.[33,34] Although graphitized MCB (GMCB) exhibits excellent conductivity, untreated MCB possesses a higher surface area and better conductivity.[35,36] This may result in a larger double-layer capacitance of the solid-state contact layer, thereby enhancing the stability of the sensor.

Screen-printed carbon electrodes (SPCEs) represent one type of all-solid-state ISE, offering unique advantages, such as flexible design, low cost, potential for mass production, and ease of handling. They are gaining increasing attention among researchers for the fabrication of solid-contact ISEs (SC-ISEs) for potentiometric detection.[37,38]

In the field of food safety, untreated MCB (purified MCB, PMCB) has not been utilized as a solid-state contact layer in constructing SC-ISEs. There are no reports of the combination of POTF and PMCB for ion detection in the literature. Traditional methods of electrode preparation have primarily focused on the detection of individual ions. Therefore, this paper proposes using a nanocomposite material based on POTF and PMCB as the solid-state contact layer for an SPCE. Upon this foundation, a multichannel SPCE capable of simultaneous detection of Na^+, K^+, Ca^{2+}, and NO_2^- ions was prepared. Characterization via chronoamperometry, impedance spectroscopy, and subsequent tests for selectivity, repeatability, reproducibility, and stability was conducted.

2. EXPERIMENTAL SECTION

2.1. Experimental Materials. Sodium ionophore (4-*tert*-butylcalix[4]arene), potassium ionophore (valinomycin), calcium ionophore ETH-129 ($C_{28}H_{48}N_2O_3$), nitrite ionophore ($C_{36}H_{46}CoN_2O_2$), PMCB, POT, poly(vinyl chloride) (PVC), tetrahydrofuran (THF), bis(2-ethylhexyl) sebacic acid (DOS), sodium tetra[3,5-bis(trifluoromethyl)phenyl]borate (NaTFPB), dimethylformamide hydroxymethyl (EDOT), decafluorooctanyl chloride, dichloromethane (CH_2Cl_2), sodium bicarbonate ($NaHCO_3$), and hexane were purchased from McLean Biochemical Technology Co., Ltd. (Shanghai, China). Deionized water with a resistivity of 18.2 mΩ·cm was

prepared by the Pall Cascada Laboratory water purification system. Other chemicals used were of analytical grade.

The four-channel screen-printed electrode (4w110) was purchased from Metrohm AG. The electrode was composed of four working carbon electrodes (2.95 mm diameter), which shared the auxiliary (carbon) and reference (silver) electrodes.

2.2. Preparation of the Solid-State Contact Layer. The stability of the solid-state contact layer substantially influences the electromotive force (EMF), posing a challenging issue that is difficult to eliminate. Many studies have focused on suppressing drift by optimizing electrode materials or developing new signal readout methods. Herein, a nanocomposite material comprising POTF and PMCB was introduced as an optimized material for the solid-state contact layer.

Before the solid-state contact layer was prepared, the SPCE was first activated by cyclic voltammetry in 0.5 M aqueous H_2SO_4 solution. The scanning range was from −1.0 to 1.0 V until stable and stable and considerable voltammetric peaks were observed. Subsequently, the SPCE was thoroughly rinsed with deionized water and dried under nitrogen gas.

In this study, we synthesized POTF containing perfluoroalkyl side chains using hydroxymethylated EDOT (95%) and perfluorodecanoyl chloride (97%) as the raw materials. The synthesis of EDOTF was performed according to a previously reported procedure, with slight modification.[39] Specifically, perfluorodecanoyl chloride (1.55 mL, 6.26 mmol/L, 1.08 equiv, 97%) was added dropwise to a solution of anhydrous CH_2Cl_2 (20 mL) containing hydroxymethylated EDOT (1.00 g, 5.80 mmol/L, 95%) and triethylamine (0.87 mL, 6.21 mmol/L, 1.07 equiv, >99%). The reaction mixture was stirred for 2.5 h, and hydrochloric acid (1 M) was added to the mixture before separating the aqueous and organic phases. The organic phase was washed with a saturated $NaHCO_3$ solution three times, and the crude product was purified by flash chromatography (hexane/CH_2Cl_2 6:4). We obtained EDOTF as a white crystalline solid, which was stored under nitrogen.

By slightly modifying the a previously reported procedure,[40] 10 mg of PMCB and 10 mg of EDOTF were added to 1 mL of POT dispersion in THF, with a concentration of 10 mg/mL. The resulting suspension was centrifuged (30 min, 7000 rpm, 30 °C), the supernatant was removed, and the precipitate was washed three times with ethanol. Subsequently, the separated solid material (hereafter termed POTF−PMCB) was dispersed in 1 mL of THF. A 10 μL aliquot of POTF−PMCB was drop-cast onto the surface of the SPCE, resulting in the prepared electrode denoted as POTF−PMCB/SPCE, which was left in the laboratory atmosphere for THF evaporation.

For comparison, ISEs using only PMCB as the solid-state contact layer were prepared. PMCB powder was dispersed in a mixture of dimethylformamide/water at a ratio of 1:1 (v/v) to a final concentration of 1 mg/mL. Specifically, 10 mg of PMCB was first immersed in 5 mL of dimethylformamide and then 5 mL of water was added, and the dispersion was sonicated at 60 kHz for 60 min. A 10 μL aliquot of PMCB was drop-cast onto the surface of the SPCE, resulting in the prepared electrode denoted as PMCB/SPCE, which was left to dry in the laboratory atmosphere.

2.3. Preparation of Multichannel Selective Electrode. By modifying the procedure reported in literature,[41,42] the composition (w/w) of the Na^+-selective membrane (Na^+-ISM) mixture was approximately 0.55% NaTFPB, 1% 4-*tert*-butylcalix[4]arene, 33% PVC, and 65.45% DOS. A total of
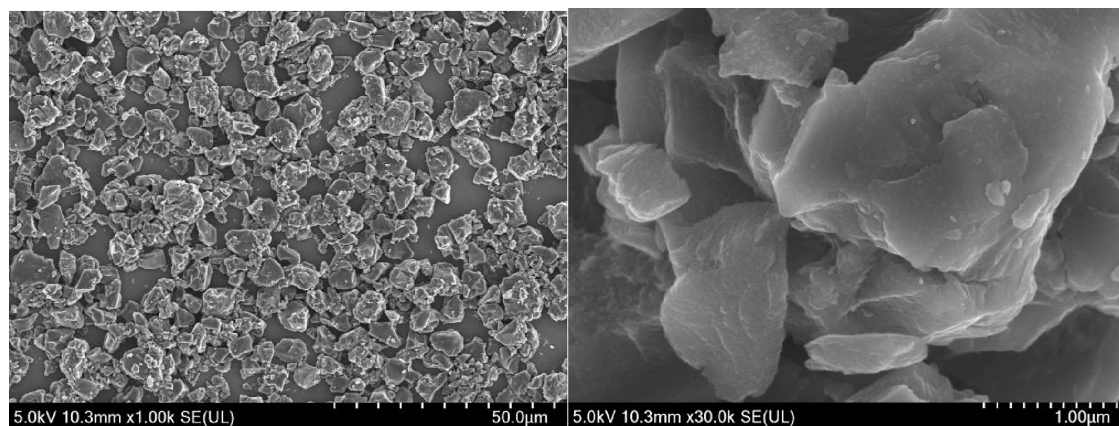
Figure 1. Image of the PMCB-ISM solid-state contact layer; right: 1 μM enlarged image.
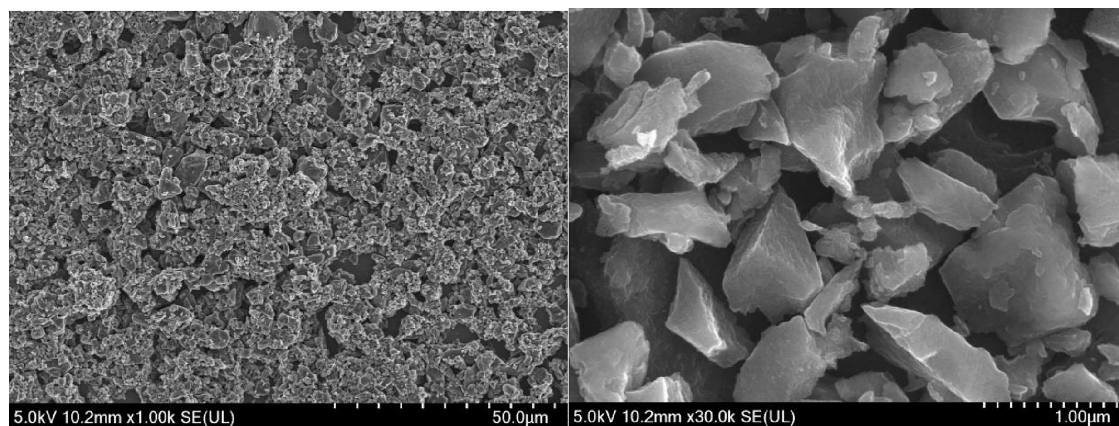

Figure 2. Image of the POTF−PMCB-ISM solid-state contact layer; right: 1 μM enlarged image.

100 mg of the mixture was dissolved in 660 μL of THF. The composition (w/w) of the K$^+$-selective membrane (K$^+$-ISM) mixture was approximately 0.5% NaTFPB, 2% valinomycin, 32.7% PVC, and 64.7% DOS. A total of 100 mg of the mixture was dissolved in 1 mL of THF. The composition (w/w) of the Ca^{2+}-selective membrane (Ca^{2+}-ISM) mixture was approximately 0.5% NaTFPB, 1% ETH-129, 33% PVC, and 65.5% DOS. A total of 100 mg of the mixture was dissolved in 1 mL of THF. The composition (w/w) of the NO$_2^-$-selective membrane NO$_2^-$-ISM) mixture was approximately 0.5% NaTFPB, 5.5% nitrite ionophore, 30.5% PVC, and 63.5% DOS. A total of 100 mg of the mixture was dissolved in 1 mL of THF.[43]

Subsequently, 10 μL each of the Na$^+$-ISM, K$^+$-ISM, Ca^{2+}-ISM, and NO$_2^-$-ISM mixtures was dropwise cast on the four working electrodes of POTF−PMCB/SPCE. The prepared multichannel screen-printed electrodes were represented as POTF−PMCB/M-SPCE. For convenience of expression, the four working electrodes are represented as POTF−PMCB/Na$^+$-SPCE, POTF−PMCB/K$^+$-SPCE, POTF−PMCB/Ca^{2+}-SPCE, and POTF−PMCB/NO$_2^-$-SPCE. For comparison, the Na$^+$-ISM mixture was dropwise cast on PMCB/SPCE and bare SPCE and the prepared electrodes are represented as PMCB/Na$^+$-SPCE and Na$^+$-SPCE, respectively. All electrodes were dried at room temperature (25 ± 2 °C). Before the test, POTF−PMCB/M-SPCE was respectively placed in 1 mM NaCl, 1 mM KCl, 1 mM CaCl$_2$, and 1 mM NaNO$_2$ for 24 h, which was the key step for the selective membrane to reach the

optimal target ion concentration and ensure the stability of the measurement potential. PMCB/Na$^+$-SPCE and Na$^+$-SPCE underwent similar operations. The adjustment step was repeated before each measurement, and all electrodes were adjusted and stored separately.

2.4. Morphological Characterization. Scanning electron microscope (SEM) images of the POTF−PMCB and PMCB solid-state contact layers were obtained using a Regulus8230 high-resolution SEM (Hitachi), and the acceleration voltage was 5 kV. The specific surface area and pore structure of the solid-state contact layer were determined using an ASAP 2460 specific surface and porosity meter. The static contact angle of water was measured using a DSA25 Drop Shape Analyzer (KRÜSS).

2.5. Electrochemical Measurement. The CHI760E electrochemical workstation was used for potential measurement at room temperature (25 °C ± 2 °C). For electrochemical impedance spectroscopy (EIS) measurements, the following parameters were used: high frequency 100 kHz, low frequency 0.01 Hz, and amplitude 10 mV. The chronopotentiometric measurement was carried out in a 10^{-3} M aqueous solution. The method involved continuously applying a constant current of +1 nA for 60 s and then applying a current of −1 nA for 60 s.

3. RESULTS AND DISCUSSION

3.1. Morphological Characterization of the Solid-State Contact Layer. Figure 1 demonstrates that the PMCB

Table 1. Pore Structure Parameters of Two Carbon Materials

carbon material	$S_{BET}(m^2/g)$	$S_{mic}(m^2/g)$	$V_{mic}(cm^3/g)$
PMCB-ISM	542.4457	77.4682	0.019873
POTF−PMCB-ISM	1414.0951	313.1374	0.111749

solid-state contact layer possessed a uniform morphology, flake structure, and large specific surface area, which could effectively enhance the ion adsorption capacity and increase the stability of the electrode potential. However, the particles in the solid-state contact layer were too large to completely cover the electrode surface. Figure 2 shows that POTF in THF dispersed PMCB, resulting in a stable suspension. Thus, the solid-state contact layer of POTF−PMCB exhibited more particles than that of PMCB, the particle size was smaller, the size distribution was more uniform, and the surface roughness was increased.

Based on the preliminary analysis of the morphology, the pore parameters of the two selected composite materials were further explored. Table 1 lists the detailed parameters of the pore structures of the two porous carbon materials. The total specific surface area (S_{BET}), micropore area (S_{mic}), and micropore volume (V_{mic}) of POTF−PMCB-ISM were greater than those of PMCB-ISM, indicating that the pore structure of POTF−PMCB-ISM was more complex. This was attributed to the aggregation of POTF and PMCB, which produced a large number of pores, making the surface rougher and strengthening the adsorption force.

The hydrophobicity of the solid-state contact layer films was evaluated using contact angle measurements. A 5 μL droplet of deionized water was deposited onto the electrode surface, and the resulting static contact angle was measured. The static contact angle of PMCB-ISM was 110.3°, which was notably increased upon blending POTF as a dispersant with PMCB to form a nanocomposite material. As shown in Figure 3, the
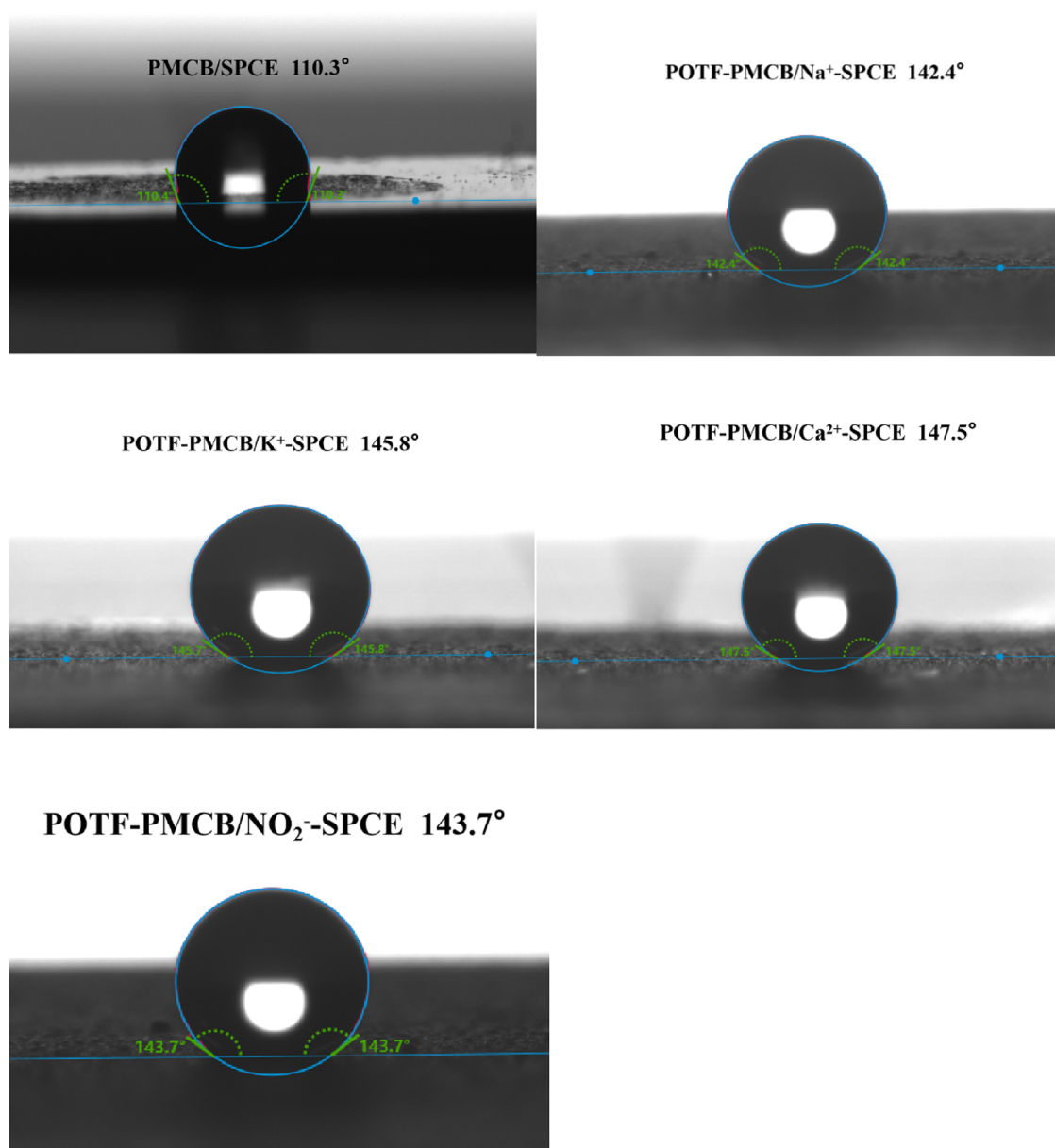
Figure 3. Static contact angle images of four working electrodes for the PMCB/SPCE and POTF−PMCB/M-SPCE.
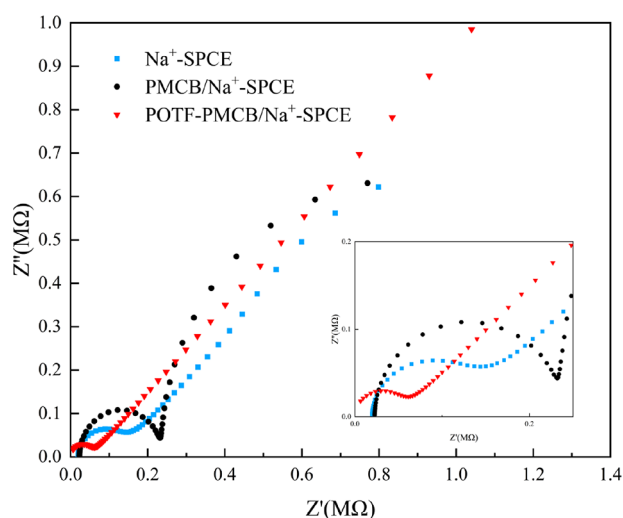
Figure 4. Electrochemical impedance spectra of POTF−PMCB/Na$^+$-SPCE, PMCB/Na$^+$-SPCE, and Na$^+$-GCE. The inset presents an enlarged view of the high-frequency region.
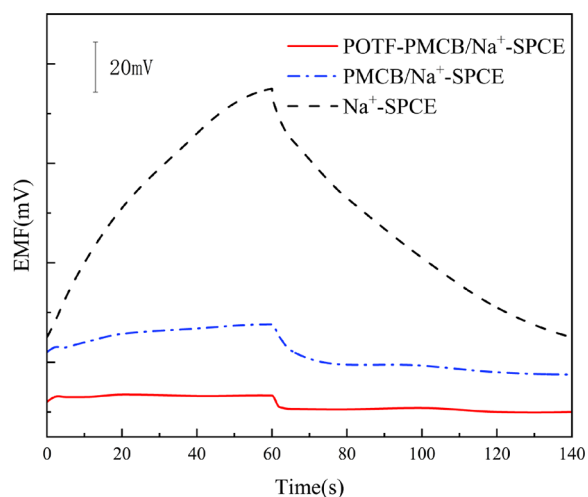

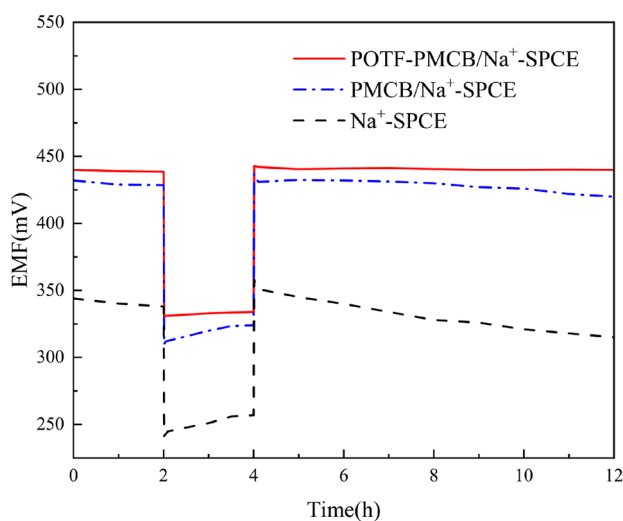**Figure 5.** Reverse chronopotentiometric curves of POTF−PMCB/Na$^+$-SPCE, PMCB/Na$^+$-SPCE, and Na$^+$-SPCE.

Figure 6. Water layer test diagram.

water contact angles of the four working electrodes of POTF−PMCB/M-SPCE were >140° and they maintained staticity for >30 min. This finding indicated that POTF−PMCB-ISM exhibited excellent hydrophobicity, making it a feasible ion-to-electron transducer for solid-state ISEs. This was primarily attributed to the intrinsic superhydrophobicity of POTF itself, along with its propensity to readily deposit onto the electrode surface. Upon fluorination, it formed a three-dimensional interconnected porous structure when combined with PMCB, leading to increased porosity and enhanced structural integrity.

3.2. Electrochemical Impedance Testing of the Solid-State Contact Layer. The electrochemical properties of POTF−PMCB/Na$^+$-SPCE, PMCB/Na$^+$-SPCE, and Na$^+$-SPCE were explored via EIS, which was conducted in a 0.1 M NaCl solution. The impedance spectra exhibited high-frequency semicircles, which was related to the volume resistance (Rbulk) of the ISE films.[44,45] The semicircular part of the higher-frequency region indicated restricted electron transfer, wherein the electron transfer resistance was equal to the diameter of the semicircle. As shown in Figure 4, the Rbulk of Na$^+$-SPCE was estimated to be 0.238 MΩ while that of PMCB/Na$^+$-SPCE decreased to 0.136 MΩ, indicating that the introduction of PMCB-ISM played a vital role in increasing the electroactive surface area. However, the Rbulk of POTF−PMCB/Na$^+$-SPCE decreased to 0.075 MΩ, indicating that POTF−PMCB, as a solid-state contact layer, could effectively enhance the charge transfer ability from ions to electrons.

3.3. Reverse Chronopotentiometric Measurement of the Solid-State Contact Layer. Chronopotentiometry was used to evaluate the effect of the applied current on the electrode. When the applied current is constant, the slope of the E−t curve (ΔE/Δt), that is, potential drift (U_{pd}), can be expressed as follows:

$$U_{pd} = \frac{\Delta E}{\Delta t} = \frac{i}{C_L} \tag{1}$$

where i is the applied current, t is the measurement time, and CL is the low-frequency capacitance of the electrode. The potential stability can be determined by the slope of the $E-t$ curve (ΔE/Δt) over a long time. The potential value of the electrode was recorded when a continuous current of 1 nA was applied. Figure 5 shows the typical chronopotentiometric curves of POTF−PMCB/Na$^+$-SPCE, PMCB/Na$^+$-SPCE, and Na$^+$-SPCE. The potential drift of POTF−PMCB/Na$^+$-SPCE was approximately 42.9 ± 1.9 μV/s, far lower than that of PMCB/Na$^+$-SPCE (144.3 ± 2.5 μV/s) and Na$^+$-SPCE (714.3 ± 25.4 μV/s). According to eq 1, the estimated capacitance value of POTF−PMCB/Na$^+$-SPCE was 23.3 μF, far greater than those of PMCB/Na$^+$-SPCE (6.93 μF) and Na$^+$-SPCE (1.39 μF). The size of the capacitance value can affect the potential stability of the electrode. The larger the capacitance value, the better its potential stability. Therefore, the prepared POTF−PMCB/Na$^+$-SPCE had better potential stability than the compared electrodes, providing a reference for the development of ISEs.

3.4. Water Layer Test of the Solid-State Contact Layer. The open-circuit potential method was used to measure the water layer performance of the electrode's solid-state contact layer. The test results are shown in Figure 6. POTF−PMCB/Na$^+$-ISE was continuously tested for open-circuit potential in a 0.1 M NaCl solution. After 2 h, the electrode was transferred to 0.1 M KCl solution for 2 h and
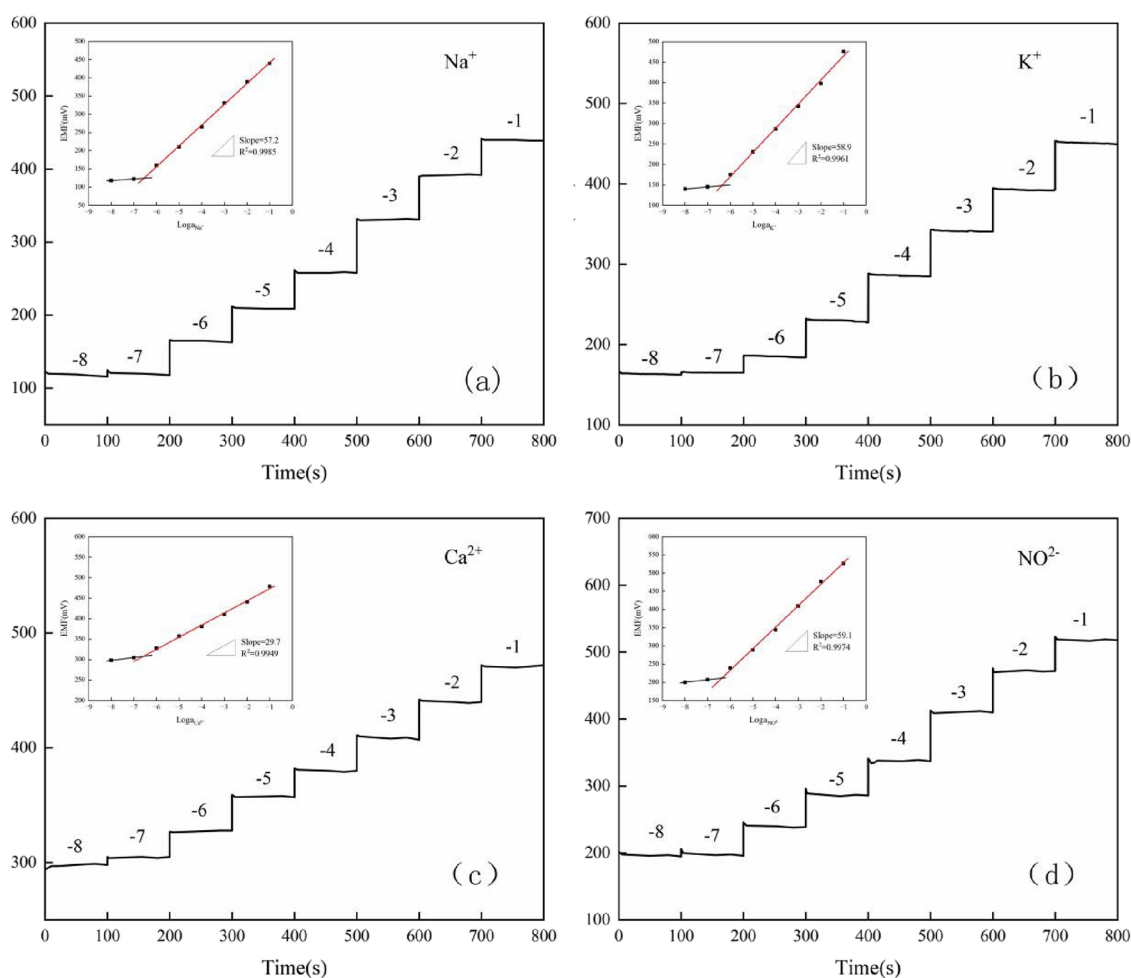
Figure 7. Potential response curves of SPCEs with the insets presenting the corresponding potential calibration diagrams: (a) POTF−PMCB/Na⁺-SPCE in NaCl solution; (b) POTF−PMCB/K⁺-SPCE in KCl solution; (c) POTF−PMCB/Ca²⁺-SPCE in CaCl₂ solution; (d) POTF−PMCB/NO₂⁻-SPCE in NaNO₂ solution.

then returned to 0.1 M NaCl solution for 8 h. As shown in Figure 6, after being transferred to a KCl solution, the potential of POTF−PMCB/Na⁺-ISE decreased sharply but the potential remained very stable. After being tested in NaCl solution, the potential of POTF−PMCB/Na⁺-ISE maintained its initial value and no substantial drift was observed relative to PMCB/Na⁺-ISE and Na⁺-ISE, confirming that the potential was stable. This indicated that the super hydrophobicity of the solid-state contact layer with POTF−PMCB could effectively avoid the appearance of an interfacial water layer, thus ensuring the excellent potential stability of the electrode.

3.5. Potential Response Measurement of the Multi-channel Selective Electrode. To evaluate the sensitivity and potential response range of the prepared POTF−PMCB/M-SPCE, the EMF was measured in $10^{-8}-10^{-1}$ M NaCl, KCl, CaCl₂, and NaNO₂ solutions, respectively. The potential time and calibration curves of POTF−PMCB/Na⁺-SPCE, POTF−PMCB/K⁺-SPCE, POTF−PMCB/Ca²⁺-SPCE, and POTF−PMCB/NO₂⁻-SPCE are presented in Figure 7a−d. Over the entire measurement process, the EMF increased with an increasing salt concentration. The slope of POTF−PMCB/Na⁺-SPCE was 57.2 ± 0.08 mV/decade (R^2 = 0.9985), which aligned with the Nernst response characteristics, and the lower limit of detection (LOD) for Na⁺ was $10^{-6.5}$ M (Figure 7a). The slope of POTF−PMCB/K⁺-SPCE was 58.9 ± 0.13 mV/

decade (R^2 = 0.9961), and the lower LOD for K⁺ was $10^{-6.4}$ M (Figure 7b). The slope of POTF−PMCB/Ca²⁺-SPCE was 29.7 ± 0.07 mV/decade (R^2 = 0.9949), and the lower LOD for Ca²⁺ was $10^{-6.7}$ M (Figure 7c). The slope of POTF−PMCB/NO₂⁻-SPCE was 59.1 ± 0.21 mV/decade (R^2 = 0.9974), and the lower LOD for NO₂⁻ was $10^{-6.3}$ M (Figure 7d). The linear response range of the four working electrodes was $10^{-6}-10^{-1}$ M (Figure 8).

Compared with other electrodes previously reported (Tables 2, 3, 4, and 5), the POTF−PMCB/SPCE exhibited a superior Nernst response and ion detection limit.

3.6. Selectivity. The selectivity coefficient, which can characterize the electrode's selective recognition ability for target ions and anti-interference ability for other ions, is an important performance parameter of ISEs. To test the anti-interference performance of POTF−PMCB/Na⁺-SPCE against other ions, 50 μg/L Na⁺ buffer was measured with interference ions K⁺, Mg²⁺, Fe³⁺, NO₃⁻, and SO₄²⁻ at the same concentration, respectively. I_s and I_0 are the oxidation peak currents of Na⁺ in the presence and absence of interfering ions, respectively. After the K⁺, Mg²⁺, Fe³⁺, NO₃⁻, and SO₄²⁻ interference ions were added, the values of I_s/I_0 were 0.964, 0.973, 0.952, 0.971, and 0.976, respectively. The relative error was <4%, and the relative standard deviation (RSD) was <2.2% (n = 3), demonstrating that POTF−PMCB/Na⁺-SPCE had
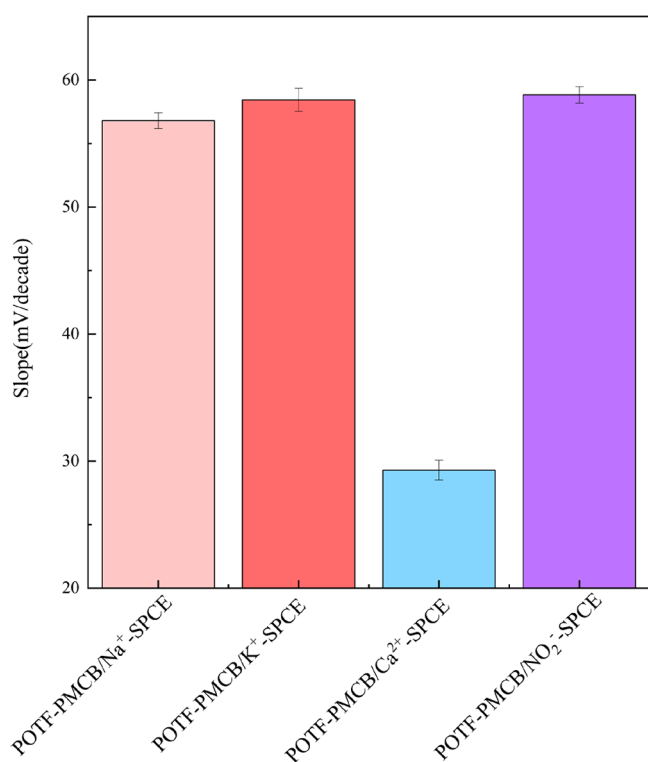
Figure 8. Histogram of response slopes of four electrodes ($n = 3$).

Table 2. Comparison with Reported Electrochemical Na$^+$ Sensors

electrode	intermediate layer/ionophore	LOD (10^{-n} M)	linear range (M)	ref
v-AuNW	v-AuNW		$10^{-3}-10^{-1}$	46
Au chip	AuNDs	6	$10^{-6}-10^{-1}$	47
paper-based	graphene		$10^{-6}-10^{-1}$	48
SPE	CS/PB		$10^{-4}-1$	49
textile screen-printed	CNT	4.9	$10^{-4}-10^{-1}$	50
SPE	CB	6.3	$10^{-4}-1$	51
flexible temporary tattoo paper	CNT	3.16	$10^{-7}-1$	52
SPCE	POTF–PMCB	6.5	$10^{-6}-10^{-1}$	this Work

Table 3. Comparison with Reported Electrochemical K$^+$ Sensors

electrode	intermediate layer/ionophore	LOD (10^{-n} M)	linear range (M)	ref
Cu	graphite–epoxy–hardener/valinomycin	4.4	$10^{-4.3}-10^{-1}$	53
Ag	N/A/PBE	4.7	$10^{-4}-10^{-1}$	54
GCE	hexanethiolate monolayer–protected gold cluster/valinomycin	6.1	$10^{-5}-10^{-1}$	55
Pt	Ppy and zeolite/valinomycin	5.1	$10^{-5}-10^{-2}$	56
GCE	MoO$_2$/valinomycin	5.5	$10^{-5}-10^{-3}$	57
carbon SPE	PANI/valinomycin	5.8	$10^{-5}-1$	58
SPCE	POTF–PMCB	6.4	$10^{-6}-10^{-1}$	this Work

Table 4. Comparison with Reported Electrochemical Ca^{2+} Sensors

electrode	intermediate layer/ionophore	LOD (10^{-n} M)	linear range (M)	ref
SPCE	rGO	5.8	$10^{-5.6}-10^{-1.6}$	59
GCE	rGO films	6.2	$10^{-5}-10^{-2.5}$	60
GCE	rGO-coated BP	5.1	$10^{-6}-10^{-1}$	61
Au	oAuCuNP MWCNTs	6.2	$10^{-6}-10^{-1}$	62
	Si/SiO$_2$/Si$_3$N$_4$	5.3	$10^{-5}-10^{-1}$	63
SPCE	PEDOT (PSS)		$10^{-4}-10^{-3}$	64
SPCE	POTF–PMCB	6.7	$10^{-6}-10^{-1}$	this Work

Table 5. Comparison with Reported Electrochemical NO$_2^-$ Sensors

electrode	intermediate layer/ionophore	LOD (10^{-n} M)	linear range (M)	ref
GCE	Ag–HNT–MoS$_2$	6.2	$10^{-4}-1$	65
GCE	Fe$_2$O$_3$–MoS$_2$	6	$10^{-6}-10^{-3}$	66
GCE	nHAP–PEDOT	4.1	$10^{-7}-10^{-3}$	67
CPE	poly(4-AB/OT)	5.5	$10^{-6}-10^{-4}$	68
GCE	PANI–MoS$_2$	5.8	$10^{-6}-10^{-3}$	69
GCE	TOSC–MoS$_2$	5.7	$10^{-6}-10^{-3}$	70
SPCE	POTF–PMCB	6.3	$10^{-6}-10^{-1}$	this Work

good selectivity for Na$^+$ (Figure S1, Supporting Information). The sensor exhibited excellent selectivity toward Na$^+$, which was attributed to the fabricated solid-state contact layer. Additionally, we employed NaTFPB, which is commonly utilized as an ion exchanger, to construct a Na$^+$-selective membrane. The performance of NaTFPB surpasses that of potassium tetrakis(4-chlorophenyl)borate (KTpClPB).[71] The response mechanism of the sensor toward Na$^+$ is depicted in Figure S2 (Supporting Information), and the ion–electron response process can be described by eq 2:[17]

$$POT^+R^-(SC) + Na^+(aq) + e^-(GC)$$
$$\rightleftharpoons POT(SC) + R^-(ISM) + Na^+(ISM) \qquad (2)$$
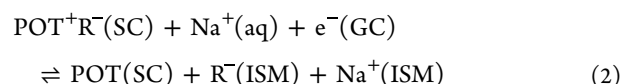
where Na$^+$(aq.) and Na$^+$(ISM) represent the concentrations in the test solution and inner solution of the ISM, respectively. The transfer of Na$^+$ occurred due to gradual oxidation of the POTF membrane to POTF$^+$.[72] Essentially, the formed POTF$^+$ paired with the anionic portion of the cation exchanger (TFPB$^-$), maintaining the system's electroneutrality, leading to the release of Na$^+$ from the ISM into the solution and the ingress of Na$^+$ from the sample into the ISM, thereby generating a response current. Meanwhile, in the solid-state contact layer, we introduced a Na$^+$ carrier that was sensitive to Na$^+$ while being insensitive to other ions, thus resulting in the preparation of a sensor with excellent selectivity.

3.7. Repeatability, Reproducibility, and Stability. Figures S3–S7 depict the performance of the prepared electrodes. To evaluate the practicability of the sensor, the repeatability, reproducibility, and long-term stability of the POTF–PMCB/Na$^+$-SPCE were also explored. Ten consecutive tests performed on the same POTF–PMCB/Na$^+$-SPCE yielded an RSD of 1.86%, indicating excellent repeatability (Figure S3). Moreover, the RSD of parallel measurement using five independent POTF–PMCB/Na$^+$-SPCE was 2.62% (Figure S4), indicating that the sensor was manufactured with high reproducibility. In addition, after a 3-week

measurement period (Figure S5), the response peak current of POTF−PMCB/Na$^+$-SPCE retained 91.2% of its initial value, with an RSD of 3.24%, demonstrating extraordinary long-term stability.

Figure S6 presents the results of the gas anti-interference test with POTF−PMCB/Na$^+$-SPCE, employing O$_2$, N$_2$, O$_2$, N$_2$, CO$_2$, and N$_2$, each for 1 h. Only a small amount of potential drift was observed during the conversion of the O$_2$ and N$_2$, and the potential was stable for the other gases.

Figure S7 presents the results of the light anti-interference test with POTF−PMCB/Na$^+$-SPCE, in which indoor light was switched to ultraviolet light once every 30 min. During the switching process, the potential remained stable, demonstrating the strong anti-interference ability of POTF−PMCB/Na$^+$-SPCE.

4. RESULTS WITH REAL SAMPLES

We employed the proposed electrode to detect Na$^+$, K$^+$, Ca^{2+}, and NO$_2^-$ in real samples. The standard addition method was

Table 6. Comparison of POTF−PMCB/M-SPCE Test Results with AAS Test Results (Mean ± Standard Deviation, $n = 3$)

iron	sample	SPCE (mmol/L)	AAS (mmol/L)	accuracy
Na$^+$	1	2.283 ± 0.03	2.335 ± 0.02	97.8%
	2	2.165 ± 0.02	2.241 ± 0.01	96.6%
	3	2.371 ± 0.02	2.415 ± 0.01	98.2%
	4	2.247 ± 0.01	2.346 ± 0.02	95.8%
	5	2.195 ± 0.03	2.327 ± 0.02	94.3%
K$^+$	1	0.114 ± 0.02	0.123 ± 0.01	92.7%
	2	0.121 ± 0.02	0.127 ± 0.01	95.3%
	3	0.127 ± 0.01	0.133 ± 0.02	95.5%
	4	0.133 ± 0.03	0.144 ± 0.02	92.4%
	5	0.111 ± 0.02	0.121 ± 0.02	91.7%
Ca^{2+}	1	0.913 ± 0.03	1.001 ± 0.02	91.2%
	2	0.845 ± 0.02	0.928 ± 0.02	91.1%
	3	0.885 ± 0.02	0.968 ± 0.01	91.4%
	4	0.987 ± 0.03	1.067 ± 0.02	92.5%
	5	0.758 ± 0.02	0.819 ± 0.02	92.6%
NO$_2^-$	1	0.157 ± 0.02	0.167 ± 0.02	94.0%
	2	0.192 ± 0.04	0.203 ± 0.03	94.6%
	3	0.122 ± 0.03	0.133 ± 0.02	91.7%
	4	0.149 ± 0.02	0.158 ± 0.04	94.3%
	5	0.175 ± 0.03	0.187 ± 0.02	93.6%

used to determine the ion concentrations in river water samples under the condition of open-circuit voltage. Five river water samples were obtained from the Zhengzhou Henan University of Technology, China. A 10 mL aliquot of sample was added to 100 mL of pure water, and the EMF was measured by POTF−PMCB/Na$^+$-SPCE after the potential stabilized, recorded as E_1. Then, 10 mL of a 1 mmol/L Na$^+$ solution was added and the measured EMF was recorded as E_2. The Na$^+$ concentration in the river water sample was calculated according to eq 3:

$$C_x = \frac{C_s V_s}{V_x}(10^{\Delta(E_2-E_1)/s} - 1)^{-1} \tag{3}$$

where C_x is the Na$^+$ concentration in river water, V_x is the volume of river water, C_s is the concentration of standard Na$^+$ solution, V_s is the volume of standard Na$^+$ solution, and S is the response slope of the electrode. K$^+$, Ca^{2+}, and NO$_2^-$

concentrations were simultaneously measured using the same method. To compare the accuracy of the detection results, atomic absorption spectroscopy (AAS) was utilized to measure the ion concentrations, and the experimental results are presented in Table 2. Using the AAS results as the standard, the accuracy of the test results was >91%, indicating that use of POTF−PMCB/M-SPCE was feasible for the simultaneous determination of complex ions in real samples (Table 6).

5. CONCLUSIONS

Herein, we present a novel multichannel solid-state ISE, utilizing POTF and PMCB modification on a SPCE. PMCB offers relevant electrochemical properties, coupled with the advantages of low cost and ease of preparation of stable dispersions. POTF, known for its excellent hydrophobicity, enhances the hydrophobic nature of the solid-state contact layer by serving as a dispersant for PMCB, eliminating the need for surfactants, and preventing the formation of a water layer. Multiple channels were designed, enabling simultaneous detection of Na$^+$, K$^+$, Ca^{2+}, and NO$_2^-$, with these ions captured by the SPCE and determined via open-circuit voltage techniques. The electrode demonstrates excellent potential stability, low LODs, and a wide linear range as well as outstanding selectivity, repeatability, and reproducibility. Moreover, the electrode's satisfactory accuracy and precision indicate the great potential of the sensor in the development of portable multi-ion field detection devices.

■ ASSOCIATED CONTENT

Ⓢ Supporting Information

The Supporting Information is available free of charge at https://pubs.acs.org/doi/10.1021/acsomega.3c10471.

> Selectivity of POTF−PMCB/Na$^+$-SPCE; response mechanism of POTF−PMCB/Na$^+$-SPCE; use the same POTF−PMCB/Na$^+$-SPCE for 10 consecutive; parallel measurements using five independent POTF−PMCB/Na$^+$-SPCEs; histogram of the response peak current of POTF−PMCB/Na$^+$-SPCE within 3 weeks; the impact of gases on sensor performance; and the impact of light on sensor performance (PDF)

■ AUTHOR INFORMATION

Corresponding Author

Yuan Zhang − *College of Information Science and Engineering, Henan University of Technology, Zhengzhou, Henan 450001, China;* Email: zy_haut@163.com

Authors

Hui Bao − *College of Information Science and Engineering, Henan University of Technology, Zhengzhou, Henan 450001, China;* ⓞ orcid.org/0009-0004-3764-6101

Jin Ye − *College of Information Science and Engineering, Henan University of Technology, Zhengzhou, Henan 450001, China; Academy of National Food and Strategic Reserves Administration, Beijing 102600, China;* ⓞ orcid.org/0000-0001-9619-4943

Complete contact information is available at: https://pubs.acs.org/10.1021/acsomega.3c10471

Notes

The authors declare no competing financial interest.

■ REFERENCES

(1) Mancia, G.; Oparil, S.; Whelton, P. K.; McKee, M.; Dominiczak, A.; Luft, F. C.; AlHabib, K.; Lanas, F.; Damasceno, A.; Prabhakaran, D.; et al. The technical report on sodium intake and cardiovascular disease in low-and middle-income countries by the joint working group of the World Heart Federation, the European Society of Hypertension and the European Public Health Association. *Eur. Heart J.* **2017**, *38* (10), 712−719.

(2) Garfinkle, M. A. Salt and essential hypertension: Pathophysiology and implications for treatment. *Journal of the American Society of Hypertension: JASH* **2017**, *11* (6), 385−391.

(3) Xue, Y.; Wen, Q.; Xu, C.; Zhang, X.; Zeng, J.; Sha, A. M.; Lan, C.; Li, L.; Wang, H.; Yang, X.; et al. Elevated salt taste threshold is associated with increased risk of coronary heart disease. *Journal of Cardiovascular Translational Research* **2020**, *13* (6), 1016−1023.

(4) Lu, J.; Zhang, H.; Hou, J.; Li, X.; Hu, X.; Hu, Y.; Easton, C. D.; Li, Q.; Sun, C.; Thornton, A. W.; et al. Efficient metal ion sieving in rectifying subnanochannels enabled by metal−organic frameworks. *Nat. Mater.* **2020**, *19* (7), 767−774.

(5) Mazzara, F.; Patella, B.; Aiello, G.; O'Riordan, A.; Torino, C.; Vilasi, A.; Inguanta, R. Electrochemical detection of uric acid and ascorbic acid using r-GO/NPs based sensors. *Electrochim. Acta* **2021**, *388*, No. 138652.

(6) Yang, Y.; Mao, J.; Yin, D.; Zhang, T.; Liu, C.; Hao, W.; Wang, Y.; Hao, J. Synergy of S-vacancy and heterostructure in BiOCl/Bi2S3− x boosting room-temperature NO₂ sensing. *Journal of Hazardous Materials* **2023**, *455*, No. 131591.

(7) Choi, M. S.; Kim, M. Y.; Mirzaei, A.; Kim, H. S.; Kim, S. I.; Baek, S. H.; Chun, D. W.; Jin, C.; Lee, K. H. Selective, sensitive, and stable NO2 gas sensor based on porous ZnO nanosheets. *Appl. Surf. Sci.* **2021**, *568*, No. 150910.

(8) Yuan, Z.; Zhao, Q.; Xie, C.; Liang, J.; Duan, X.; Duan, Z.; Li, S.; Jiang, Y.; Tai, H. Gold-loaded tellurium nanobelts gas sensor for ppt-level NO₂ detection at room temperature. *Sens. Actuators, B* **2022**, *355*, No. 131300.

(9) Chaneam, S.; Taweetong, W.; Kaewyai, K.; Thienwong, P.; Takaew, A.; Chaisuksant, R. Fabrication of a nitrate selective electrode for determination of nitrate in fertilizers by using flow injection analysis system. *Procedia Chemistry* **2016**, *20*, 73−75.

(10) Li, G.; Qi, X.; Wu, J.; Wan, X.; Wang, T.; Liu, Y.; Chen, Y.; Xia, Y. Highly stable electrochemical sensing platform for the selective determination of pefloxacin in food samples based on a molecularly imprinted-polymer-coated gold nanoparticle/black phosphorus nanocomposite. *Food Chem.* **2024**, *436*, No. 137753.

(11) Fan, Y.; Xu, C.; Wang, R.; Hu, G.; Miao, J.; Hai, K.; Lin, C. Determination of copper (II) ion in food using an ionic liquids-carbon nanotubes-based ion-selective electrode. *Journal of Food Composition and Analysis* **2017**, *62*, 63−68.

(12) Cuartero, M.; Ruiz, A.; Galián, M.; Ortuño, J. A. Potentiometric electronic tongue for quantitative ion analysis in natural mineral waters. *Sensors* **2022**, *22* (16), 6204.

(13) Li, G.; Wan, X.; Xia, Y.; Tuo, D.; Qi, X.; Wang, T.; Mehmandoust, M.; Erk, N.; He, Q.; Li, Q. Lamellar α-Zirconium phosphate nanoparticles supported on N-doped graphene nanosheets as electrocatalysts for the detection of levofloxacin. *ACS Applied Nano Materials* **2023**, *6* (18), 17040−17052.

(14) Shao, Y.; Ying, Y.; Ping, J. Recent advances in solid-contact ion-selective electrodes: Functional materials, transduction mechanisms, and development trends. *Chem. Soc. Rev.* **2020**, *49* (13), 4405−4465.

(15) Özer, T. Low-cost pencil-graphite multi-electrodes for simultaneous detection of iron and copper. *Journal of the Turkish Chemical Society Section A: Chemistry* **2022**, *9* (1), 1−12.

(16) Das, P.; Mondal, S.; Malik, S. Fully organic polyaniline nanotubes as electrode material for durable supercapacitor. *Journal of Energy Storage* **2021**, *39*, No. 102662.

(17) Lyu, Y.; Gan, S.; Bao, Y.; Zhong, L.; Xu, J.; Wang, W.; Liu, Z.; Ma, Y.; Yang, G.; Niu, L. Solid-contact ion-selective electrodes: Response mechanisms, transducer materials and wearable sensors. *Membranes* **2020**, *10* (6), 128.

(18) Liu, H.; Gu, Z.; Zhao, Q.; Li, S.; Ding, X.; Xiao, X.; Xiu, G. Printed circuit board integrated wearable ion-selective electrode with potential treatment for highly repeatable sweat monitoring. *Sens. Actuators, B* **2022**, *355*, No. 131102.

(19) Wardak, C.; Pietrzak, K.; Morawska, K.; Grabarczyk, M. Ion-selective electrodes with solid contact based on composite materials: A review. *Sensors* **2023**, *23* (13), 5839.

(20) Zhang, Y.; Tao, Y.; Wang, K.; Zhao, S.; Zhu, J.; Cheng, H. Two kinds of polyaniline fiber photo sensor with interdigital electrode and flexible hydrogel. *J. Appl. Polym. Sci.* **2021**, *138* (26), 50628.

(21) Hu, J.; Stein, A.; Bühlmann, P. Rational design of all-solid-state ion-selective electrodes and reference electrodes. *TrAC Trends in Analytical Chemistry* **2016**, *76*, 102−114.

(22) Wan, X.; Du, H.; Tuo, D.; Qi, X.; Wang, T.; Wu, J.; Li, G. Uio-66/carboxylated multiwalled carbon nanotube composites for highly efficient and stable voltammetric sensors for gatifloxacin. *ACS Applied Nano Materials* **2023**, *6* (20), 19403−19413.

(23) Li, G.; Xia, Y.; Tian, Y.; Wu, Y.; Liu, J.; He, Q.; Chen, D. Recent developments on graphene-based electrochemical sensors toward nitrite. *J. Electrochem. Soc.* **2019**, *166* (12), B881.

(24) Xue, M.; Mackin, C.; Weng, W. H.; Zhu, J.; Luo, Y.; Luo, S. X. L.; Lu, A. Y.; Hempel, M.; McVay, E.; Kong, J.; Palacios, T. Integrated biosensor platform based on graphene transistor arrays for real-time high-accuracy ion sensing. *Nat. Commun.* **2022**, *13* (1), 5064.

(25) Hassan, S. S. M.; Kamel, A. H.; Amr, A. E. G. E.; Hashem, H. M.; Bary, E. M. A. Imprinted polymeric beads-based screen-printed potentiometric platforms modified with multi-walled carbon nanotubes (MWCNTs) for selective recognition of fluoxetine. *Nanomaterials* **2020**, *10* (3), 572.

(26) Pechenkina, I. A.; Mikhelson, K. N. Materials for the ionophore-based membranes for ion-selective electrodes: Problems and achievements (review paper). *Russian Journal of Electrochemistry* **2015**, *51* (2), 93−102.

(27) Hambly, B.; Guzinski, M.; Pendley, B.; Lindner, E. Evaluation, pitfalls and recommendations for the "water layer test" for solid contact ion-selective electrodes. *Electroanalysis* **2020**, *32* (4), 781−791.

(28) Asthana, A.; Maitra, T.; Büchel, R.; Tiwari, M. K.; Poulikakos, D. Multifunctional superhydrophobic polymer/carbon nanocomposites: Graphene, carbon nanotubes, or carbon black? *ACS Appl. Mater. Interfaces* **2014**, *6* (11), 8859−8867.

(29) Carey, J. L., III; Hirao, A.; Sugiyama, K.; Bühlmann, P. Semifluorinated polymers as ion-selective electrode membrane matrixes. *Electroanalysis* **2017**, *29* (3), 739−747.

(30) Paczosa-Bator, B. Effects of type of nanosized carbon black on the performance of an all-solid-state potentiometric electrode for nitrate. *Microchimica Acta* **2014**, *181* (9−10), 1093−1099.

(31) Pacheco, M. R.; Barbosa, S. C.; Quadrado, R. F. N.; Fajardo, A. R.; Dias, D. Glassy carbon electrode modified with carbon black and cross-linked alginate film: A new voltammetric electrode for paraquat determination. *Anal. Bioanal. Chem.* **2019**, *411* (15), 3269−3280.

(32) Rahman, M.; Alam, M.; Asiri, A. M. Carbon black co-adsorbed ZnO nanocomposites for selective benzaldehyde sensor development by electrochemical approach for environmental safety. *Journal of Industrial and Engineering Chemistry* **2018**, *65*, 300−308.

(33) Mehdipour-Ataei, S.; Aram, E. Mesoporous carbon-based materials: A review of synthesis, modification, and applications. *Catalysts* **2023**, *13* (1), 2.

(34) Zhang, P.; Zhang, J.; Dai, S. Mesoporous carbon materials with functional compositions. *Chemistry* **2017**, *23* (9), 1986−1998.

(35) Feng, Y.-Y.; Chen, Y.; Wang, Z.; Wei, J. Synthesis of mesoporous carbon materials from renewable plant polyphenols for environmental and energy applications. *New Carbon Materials* **2022**, *37* (1), 196−222.

(36) Benzigar, M. R.; Talapaneni, S. N.; Joseph, S.; Ramadass, K.; Singh, G.; Scaranto, J.; Ravon, U.; Al-Bahily, K.; Vinu, A. Recent advances in functionalized micro and mesoporous carbon materials: synthesis and applications. *Chem. Soc. Rev.* **2018**, *47* (8), 2680−2721.

(37) Li, L.; Chen, B.; Luo, L.; Liu, X.; Bi, X.; You, T. Sensitive and selective detection of Hg²⁺ in tap and canal water via self-enhanced ECL aptasensor based on NH₂⁻Ru@ SiO₂⁻NGQDs. *Talanta* **2021**, *222*, No. 121579.

(38) Parrilla, M.; Cuartero, M.; Crespo, G. A. Wearable potentiometric ion sensors. *TrAC Trends in Analytical Chemistry* **2019**, *110*, 303−320.

(39) Papp, S.; Bojtár, M.; Gyurcsányi, R. E.; Lindfors, T. Potential reproducibility of potassium-selective electrodes having perfluorinated alkanoate side chain functionalized poly(3,4-ethylenedioxytiophene) as a hydrophobic solid contact. *Anal. Chem.* **2019**, *91* (14), 9111−9118.

(40) Kałuża, D.; Jaworska, E.; Mazur, M.; Maksymiuk, K.; Michalska, A. Multiwalled carbon nanotubes-poly(3-octylthiophene-2,5-diyl) nanocomposite transducer for ion-selective electrodes: Raman spectroscopy insight into the transducer/membrane interface. *Anal. Chem.* **2019**, *91* (14), 9010−9017.

(41) Gao, W.; Emaminejad, S.; Nyein, H. Y. Y.; Challa, S.; Chen, K.; Peck, A.; Fahad, H. M.; Ota, H.; Shiraki, H.; Kiriya, D.; et al. Fully integrated wearable sensor arrays for multiplexed in situ perspiration analysis. *Nature* **2016**, *529* (7587), 509−514.

(42) Kim, M. Y.; Lee, J. W.; Park, D. J.; Lee, J. Y.; Myung, N. V.; Kwon, S. H.; Lee, K. H. Highly stable potentiometric sensor with reduced graphene oxide aerogel as a solid contact for detection of nitrate and calcium ions. *J. Electroanal. Chem.* **2021**, *897*, No. 115553.

(43) Soares, R. R. A.; Hjort, R. G.; Pola, C. C.; Jing, D.; Cecon, V. S.; Claussen, J. C.; Gomes, C. L. Ion-selective electrodes based on laser-induced graphene as an alternative method for nitrite monitoring. *Microchim. Acta* **2023**, *190* (1), 43.

(44) Crespo, G. A.; Macho, S.; Rius, F. X. Ion-selective electrodes using carbon nanotubes as ion-to-electron transducers. *Anal. Chem.* **2008**, *80* (4), 1316−1322.

(45) Konopka, A.; Sokalski, T.; Michalska, A.; Lewenstam, A.; Maj-Zurawska, M. Factors affecting the potentiometric response of all-solid-state solvent polymeric membrane calcium-selective electrode for low-level measurements. *Anal. Chem.* **2004**, *76* (21), 6410−6418.

(46) Zhai, Q.; Yap, L. W.; Wang, R.; Gong, S.; Guo, Z.; Liu, Y.; Lyu, Q.; Wang, J.; Simon, G. P.; Cheng, W. Vertically aligned gold nanowires as stretchable and wearable epidermal ion-selective electrode for noninvasive multiplexed sweat analysis. *Analytical chemistry* **2020**, *92* (6), 4647−4655.

(47) Wang, S.; Wu, Y.; Gu, Y.; Li, T.; Luo, H.; Li, L. H.; Bai, Y.; Li, L.; Liu, L.; Cao, Y.; Ding, H.; Zhang, T. Wearable sweatband sensor platform based on gold nanodendrite array as efficient solid contact of ion-selective electrode. *Analytical chemistry* **2017**, *89* (19), 10224−10231.

(48) An, Q.; Gan, S.; Xu, J.; Bao, Y.; Wu, T.; Kong, H.; Zhong, L.; Ma, Y.; Song, Z.; Niu, L. A multichannel electrochemical all-solid-state wearable potentiometric sensor for real-time sweat ion monitoring. *Electrochem. Commun.* **2019**, *107*, No. 106553.

(49) Ghosh, T.; Das, A.; König, B. Photocatalytic N-formylation of amines via a reductive quenching cycle in the presence of air. *Organic and Biomolecular Chemistry* **2017**, *15* (12), 2536−2540.

(50) Parrilla, M.; Cánovas, R.; Jeerapan, I.; Andrade, F. J.; Wang, J. A textile-based stretchable multi-ion potentiometric sensor. *Adv. Healthcare Mater.* **2016**, *5* (9), 996−1001.

(51) Mazzaracchio, V.; Serani, A.; Fiore, L.; Moscone, D.; Arduini, F. All-solid state ion-selective carbon black-modified printed electrode for sodium detection in sweat. *Electrochim. Acta* **2021**, *394*, No. 139050.

(52) Roy, S.; David-Pur, M.; Hanein, Y. Carbon nanotube-based ion selective sensors for wearable applications. *ACS Appl. Mater. Interfaces* **2017**, *9* (40), 35169−35177.

(53) Vardar, G.; Altikatoğlu, M.; Ortaç, D.; Cemek, M.; Işildak, İ Measuring calcium, potassium, and nitrate in plant nutrient solutions using ion-selective electrodes in hydroponic greenhouse of some vegetables. *Biotechnology and Applied Biochemistry* **2015**, *62* (5), 663−668.

(54) Siswanta, D.; Wulandari, Y. D.; Jumina, J. Synthesis of poly(benzyleugenol) and its application as an ionophore for a potassium ion-selective electrode. *EurAsian J. Anal. Chem.* **2016**, *11* (2), 115−125.

(55) An, Q.; Jiao, L.; Jia, F.; Ye, J.; Li, F.; Gan, S.; Zhang, Q.; Ivaska, A.; Niu, L. Robust single-piece all-solid-state potassium-selective electrode with monolayer-protected Au clusters. *J. Electroanal. Chem.* **2016**, *781*, 272−277.

(56) Yu, K.; He, N.; Kumar, N.; Wang, N.; Bobacka, J.; Ivaska, A. Electrosynthesized polypyrrole/zeolite composites as solid contact in potassium ion-selective electrode. *Electrochim. Acta* **2017**, *228*, 66−75.

(57) Zeng, X.; Qin, W. A solid-contact potassium-selective electrode with MoO2 microspheres as ion-to-electron transducer. *Anal. Chim. Acta* **2017**, *982*, 72−77.

(58) Tran, T. N. T.; Qiu, S.; Chung, H. J. Potassium ion selective electrode using polyaniline and matrix-supported ion-selective PVC membrane. *IEEE Sensors Journal* **2018**, *18* (22), 9081−9087.

(59) Ping, J.; Wang, Y.; Ying, Y.; Wu, J. Application of electrochemically reduced graphene oxide on screen-printed ion-selective electrode. *Anal. Chem.* **2012**, *84* (7), 3473−3479.

(60) Hernández, R.; Riu, J.; Bobacka, J.; Vallés, C.; Jiménez, P.; Benito, A. M.; Maser, W. K.; Rius, F. X. Reduced graphene oxide films as solid transducers in potentiometric all-solid-state ion-selective electrodes. *J. Phys. Chem. C* **2012**, *116* (42), 22570−22578.

(61) Yang, Q.; Zhang, M.; Ming, C.; Liu, G.; Wang, M. All-solid-state Ca ion-selective electrode with black phosphorus and reduced graphene oxide as the mediator layer. *Int. J. Electrochem. Sci.* **2019**, *14* (6), 4933−4945.

(62) Liu, Y.; Liu, Y.; Yan, R.; Gao, Y.; Wang, P. Bimetallic AuCu nanoparticles coupled with multi-walled carbon nanotubes as ion-to-electron transducers in solid-contact potentiometric sensors. *Electrochim. Acta* **2020**, *331*, No. 135370.

(63) Ermolenko, Y.; Yoshinobu, T.; Mourzina, Y.; Schöning, M. J.; Vlasov, Y.; Iwasaki, H. The Hybrid K⁺/Ca²⁺ Sensor Based on Laser Scanned Silicon Transducer for Multi-component Analysis. *Anal. Sci./Suppl.* **2002**, *17*, i777−i780.

(64) Wang, Y.; Xu, H.; Yang, X.; Luo, Z.; Zhang, J.; Li, G. All-solid-state blood calcium sensors based on screen-printed poly (3, 4-ethylenedioxythiophene) as the solid contact. *Sens. Actuators, B* **2012**, *173*, 630−635.

(65) Ghanei-Motlagh, M.; Taher, M. A. A novel electrochemical sensor based on silver/halloysite nanotube/molybdenum disulfide nanocomposite for efficient nitrite sensing. *Biosens. Bioelectron.* **2018**, *109*, 279−285.

(66) Wang, H.; Chen, P.; Wen, F.; Zhu, Y.; Zhang, Y. Flower-like Fe2O3@MoS2 nanocomposite decorated glassy carbon electrode for the determination of nitrite. *Sens. Actuators, B* **2015**, *220*, 749−754.

(67) Wang, G.; Han, R.; Feng, X.; Li, Y.; Lin, J.; Luo, X. A glassy carbon electrode modified with poly (3, 4-ethylenedioxythiophene) doped with nano-sized hydroxyapatite for amperometric determination of nitrite. *Microchimica Acta* **2017**, *184*, 1721−1727.

(68) Norouzi, B.; Rajabi, M. Fabrication of poly(4-aminobenzoic acid/o-toluidine) modified carbon paste electrode and its electrocatalytic property to the oxidation of nitrite. *J. Anal. Chem.* **2017**, *72* (8), 897−903.

(69) Zhang, Y.; Chen, P.; Wen, F.; Huang, C.; Wang, H. Construction of polyaniline/molybdenum sulfide nanocomposite: Characterization and its electrocatalytic performance on nitrite. *Ionics* **2016**, *22* (7), 1095−1102.

(70) Wang, Q.; Ma, S.; Huang, H.; Cao, A.; Li, M.; He, L. Highly sensitive and selective spectrofluorimetric determination of nitrite in food products with a novel fluorogenic probe. *Food Control* **2016**, *63*, 117−121.

(71) Sato, H.; Wakabayashi, M.; Ito, T.; Sugawara, M.; Umezawa, Y. Potentiometric responses of ionophore-incorporated bilayer lipid membranes with and without added anionic sites. *Anal. Sci.* **1997**, *13* (3), 437−446.

(72) Yuan, D. J.; Cuartero, M.; Crespo, G. A.; Bakker, E. voltammetric thin-layer ionophore-based films: Part 1. Experimental evidence and numerical simulations. *Anal. Chem.* **2017**, *89* (1), 586−594.